REUSABLE SOLID ROCKET MOTOR NOZZLE JOINT -4 THERMAL ANALYSIS

J. Louie Clayton
National Aeronautics and Space Administration
Marshall Space Flight Center
Huntsville, Alabama

Abstract

This study provides for development and test verification of a thermal model used for prediction of joint heating environments, structural temperatures and seal erosions in the Space Shuttle Reusable Solid Rocket Motor (RSRM) Nozzle Joint-4. The heating environments are a result of rapid pressurization of the joint free volume assuming a leak path has occurred in the filler material used for assembly gap close out. Combustion gasses flow along the leak path from nozzle environment to joint O-ring gland resulting in local heating to the metal housing and erosion of seal materials. Analysis of this condition was based on usage of the NASA Joint Pressurization Routine (JPR) for environment determination and the Systems Improved Numerical Differencing Analyzer (SINDA) for structural temperature prediction. Model generated temperatures, pressures and seal erosions are compared to hot fire test data for several different leak path situations. Investigated in the hot fire test program were nozzle joint-4 O-ring erosion sensitivities to leak path width in both open and confined joint geometries. Model predictions were in generally good agreement with the test data for the confined leak path cases. Worst case flight predictions are provided using the test-calibrated model. Analysis issues are discussed based on model calibration procedures.

List of Symbols

A	normal surface area
C	specific heat
D	passage hydraulic
e	Euler constant
f	Moody friction factor
g_c	gravitational constant
h	convection film coefficient
H	enthalpy
L	flow path length
M	molecular weight
m	mass
p	pressure
Q	heat rate
R	gas constant
T	temperature
U	internal energy
t	time
V	volume
W	work

Greek

Δ	difference operator

Subscripts

g	gas
i	inlet
o	outlet
p	constant pressure
w	wall
v	constant volume

Summary

First, an overview of the RSRM nozzle joint-4 configuration and process history will be presented. JPR[1] methodology fundamentals are covered next by providing a cursory look at governing equations and modeling techniques used for computation of heating environments. Incorporation with SINDA[2] as a finite element thermal solver is briefly discussed. Results of model calibration with data obtained from test program "ETP-1385 Joint-4 Hot Gas Test"[3] are discussed. Finally, the test calibrated joint-4 model will be used for prediction of worst case flight results using nozzle joint-4 boundary conditions and current gland geometry. In closing analysis issues, results and conclusions are presented.

Introduction

Nozzle Joint-4 Information

RSRM Nozzle Joint-4, Fig. 1, is located aft of the throat in the supersonic region of the nozzle. Liner materials at this location are a carbon phenolic ablator backed by glass phenolic insulator, which is secondarily bonded to a steel housing. Operational environments are estimated to be ~150 psia static pressure at a local recovery temperature of ~5100°R. The primary O-ring is a face seal housed in a glass phenolic gland and the opposing sealing surface is the aft end of the steel throat assembly. The joint-4 secondary O-ring is a bore seal and contained entirely in the aft end of the throat housing structure.

Contributions to joint free volume come from the primary and secondary gland, the chamfer region and assembly gaps in the liner materials. After the housings are bolted together, the assembly gaps are back-filled with room temperature vulcanizing silicon (RTV). The RTV is injected radially penetrating the length of the assembly gap typically with depth irregularities adjacent to the primary O-ring gland. Post-flight observation of typical RTV penetration depths has allowed for an average assembly gap volume contribution to be estimated at ~0.5 in^3. Nominal primary gland volume is ~2.2 in^3, chamfer region is estimated at 5.5 in^3 and secondary gland has a nominal volume of ~4.2 in^3. As an assembly aid HD-2 grease is applied to mating surfaces and has the effect of a volume filler. Based on the post-flight data, about one cubic inch of grease typically occupies joint volume. Accounting for all individual contributions, total joint-4 free volume on a nominal basis is about 11.4 in^3.
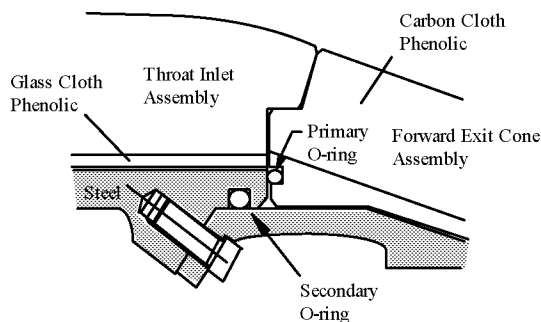

Fig. 1. RSRM Nozzle Joint–4 Cross Section

Nozzle Joint Back-Fill Process

There are two ways of dealing with assembly gaps that can potentially communicate motor environments with joint sealing surfaces. The first is to vent the joint. No back-fill materials are used in the gaps. Pressurization of the primary gland is rapid and heating to the sealing surfaces a result of compression of the gases at the stagnation point. This design is used in many solid rocket motor joints with perhaps addition of a permeable "slag barrier" to trap hot particulate matter. The second method fills the assembly gaps with a "filler" material, which is the process used in the RSRM program. Early in the motor program, application of RTV was a one-step procedure involving radial injection into the assembly gap. The procedure had the characteristic of producing "tail voids" at the circumferential location where the injection process began. It was determined voids were a result of the close-out phase of the back-fill process. When the injection process clocked 360 degrees and was "closing-out", air was being trapped and compressed. Over time the trapped air would work its way out of the joint through the uncured RTV. Tail voids are formed extending from gland inboard to flame surface. If the void terminates before it reaches the free surface, it has potential for being exposed during motor operation. For this scenario, a confined leak path pressurizes the primary gland usually resulting in local heat affects and seal erosion. This specific anomaly happened in nozzle joint-3 of motor flight sets 44 and 45 where minor amounts of primary seal erosion occurred.

Programmatic evolution of the back-fill process has led to qualification of a two-step procedure. The joint gaps are filled, partially excavated, and then re-filled. Due to the geometry involved in joint-4, the excavation (a digging process) is performed to the first turn. The excavated portion of the gap is then re-filled with RTV. A vacuum close-out procedure is used to minimize trapped air. This process change transpired on RSRM-48 nozzle flight set and since that time, there has been no evidence of gas penetration into the joints as a result of a tail void.

A problem with the current procedure is that excavation can only be performed in the first leg to the inflection point. If a void exists in the second leg of the assembly gap, there is a finite chance of exposure resulting in a confined jet pressurization of the primary gland. Based on

liner char/erosion statistics at this nozzle station, the 3-σ char line passes the inflection point at ~104 seconds into motor operation. At this time chamber pressures are over 400 psia - thus there is potential for primary seal damage should this condition occur.

Gas Dynamic/ Thermal Modeling

Environment Prediction

Determination of the pressurization-heating environment was accomplished with the NASA JPR computer program. Calculation strategy is based on a detail inlet simulation (leak path) connected to a pressurizing volume (O-ring gland). This scheme has sufficed for the majority of gland filling problems due to characteristics of the heat transfer and influence on the overall pressurization transient. Most heat transfer occurs near the inlet while gland pressurization takes place with relatively cool gasses. The JPR method is efficient in terms of nodalization in that a detail grid is used to resolve thermal gradients where necessary and a course grid where heat transfer is not as significant. The JPR numerical scheme is based on a resistor-capacitor (R-C) formulated flow network, Fig. 2, which solves concurrently with a detail SINDA conduction grid. This scheme allows for flow-thermal-structural couplings to be simulated.

JPR uses the Lapple Tables[4] for computation of compressible gas flow rates based on flow path inlet-exit conditions. The basic form of the flow equation for constant area is given as;

$$\dot{m} = p_i A \sqrt{\frac{g_c M}{e R T_i}} f(\frac{L}{D}, \frac{p_o}{p_i}) \qquad (1)$$

where; $f(\frac{L}{D}, \frac{p_o}{p_i})$ is a table lookup factor

During the volume filling process, instantaneous values of inlet-exit pressure and temperature constitute the known conditions of the state variables in Eq. (1). Evaluation of flow rates by this method assumes that pressure and friction forces control flow rate magnitude at any instant in time (quasi-steady solution).

The limitation of constant flow path area in Eq. (1) necessitated formulation of a procedure that solves for a system of connected paths. By applying continuity of mass and energy at path inlet-exit, Eq. (1) expands into a system of equations that can be solved simultaneously to describe the system flow rate. This method of solution allows for inclusion of secondary head loss terms such as turns, expansion/contractions in proper serial order in the direction of flow.
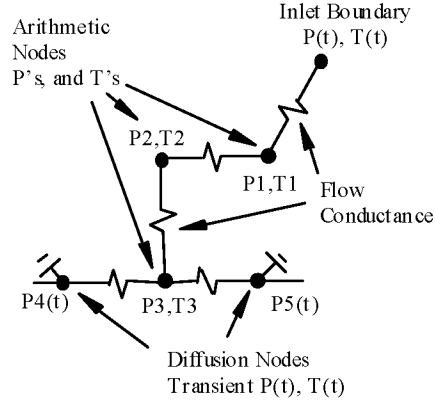

Fig. 2. Gas Flow R-C Network Formulation

Calculations of the thermodynamic conditions in the volumes are based on bulk formulation of the unsteady form of the mass and energy conservation equations. They are given as:

$$\frac{dm}{dt} = (\dot{m}_i - \dot{m}_o) \qquad (2)$$

$$\dot{Q} + H_i = \frac{d}{dt}(mU) + H_o + W \qquad (3)$$

where; $\dot{Q} = \bar{h}A(T_g - T_w)$

$$\Delta U = C_v \Delta T$$

$$\Delta H = C_p \Delta T$$

$$pV = mRT \qquad (4)$$

Eqs. (2) and (3) are finite differenced by fully implicit methods and applied to the number of volumes involved in the simulation. Temperature and composition dependent specific heats are used for enthalpy and internal energy terms in Eq. (3). Gas compositional chemistry was assumed frozen below 2500°F and in equilibrium above this value. Aluminum Oxide (Al₂O₃) contributions to mixture properties were excluded below 3700°F. There was no attempt at modeling constituent deposition along the flow path. The ideal gas law, Eq. (4), was used

3

to relate total pressure to volumetric mass and bulk temperature. Equivalent molecular weights were used in the evaluation of the gas constant.

JPR internally solves for volumetric heat loss by using convective boundary conditions coupled to a 1-D conduction grid. The built-in conduction grid allows for efficient calculation of heat loss in gland regions away from the leak path inlet. Details of JPR computational procedures are found in Ref. [1].

Detail Temperature Prediction

A feature of JPR is the concurrent solution of a detail conduction grid describing heat transfer along the inlet leak path. For this study a 3-D finite element grid, Fig. 3., was constructed using MSC/PATRAN[5]. The grid region contained thermal mass sufficient to capture the heat transfer events associated with joint pressurization. Along the inlet to the primary gland, heat losses to the lateral sides were sub-modeled with a finite difference grid. Lateral heat transfer (z-direction) was accounted for and a numerically simplified treatment of flow path ablation easily implemented. Given path rectangular aspect ratio's and duration of a typical filling event, conduction corner effects have a second order influence on gas temperature prediction.
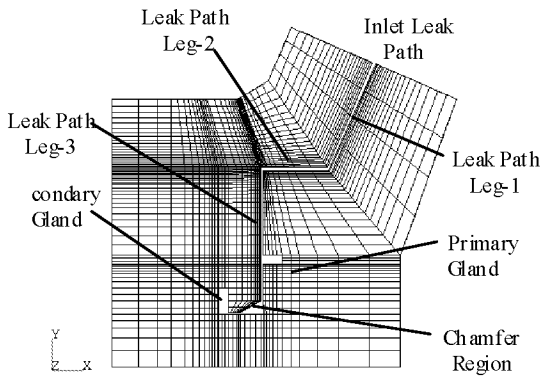

Fig. 3. Nozzle Joint-4 Finite Element Grid

Conductivity and heat capacitances for liner materials were temperature and density dependent. The material was assumed to be fully charred at temperatures above 1000°F and no accounting for kinetic decomposition rate was considered. Directional conductivites were used and ply angles fixed at 45° from nozzle centerline. Steel and O-ring material properties were input as

functions of temperature. The O-ring material is elastomeric fluorocarbon (V1115) and has an ablation temperature of ~805°F. Surface erosion rates have been measured[6] and correlated in terms of heat transfer coefficient. Model predictions of O-ring erosion are performed on a fine grid sub-model using internally calculated environments and the 1-D surface erosion data.

Jet Spreading and Computational Fluid Dynamics (CFD) Sub-Modeling

Several test configurations include regions where the leak path is not confined. The flow is free to spread laterally before entering an O-ring gland. Several of the primary gland tests were configured with leg-3 open over the length of the article. Gas flows along a confined rectangular path in legs-1 and -2 and enters the unconfined leg-3 where a partial free jet forms. The width of the jet increases and centerline velocity decreases in the direction of flow[7]. There is a generally a reduction in centerline mass velocity accompanied by lower gas temperatures at the impingement point.

For the secondary gland cases, jet spreading occurs in the chamfer region outboard of the primary seal. Leakage past the primary seal will result in pressurization of both chamfer and secondary gland. Assuming flow past a leaking primary is localized, flow enters the chamfered region and spreads laterally before entering the secondary gland. It was determined by CFD analysis most of the flow traverses the chamfer paths before entering the secondary groove. Three-dimensional CFD models of both leg-3 and joint chamfer-secondary regions were constructed using the Finite Difference Navier-Stokes (FDNS 3-D) code.[8]

An approximate method of quantifying relative amounts of flow involved in heat transfer in a spreading region was devised and based on CFD sub-modeling. The rate of gland pressurization and inlet mass flow can be sufficiently calculated with traditional 1-D internal flow equations. Spreading regions are treated as a secondary loss (sudden expansion) in the global flow solution. The globally computed mass flow, temperature and pressure of gas entering a spreading region provide in-flow boundary conditions for a CFD sub-model. The technique involves capturing time slices of the inlet conditions and performing steady CFD solutions of the flow field. Results are tabulated where the dependent variable is the ratio of centerline mass velocity versus mass flow rate

and distance from origin of jet. This method of correlation is incorporated into a transient SINDA thermal model to determine time based flow fractions used in specific locations of the conduction grid.

Results

Work performed under Engineering Test Plan (ETP)-1385 "Tortuous Path Thermal Test Bed" generated usable results for most testing performed. Early tests were developmental in nature and results considered not highly reliable. Fig. 4 depicts a cross section of the test article showing centerline measurement locations.
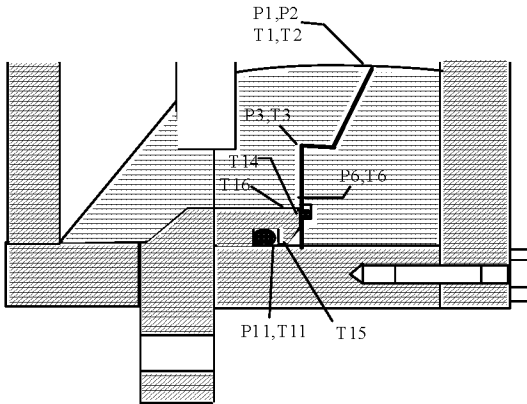
Fig. 4. Test Article Measurement Locations

The assembly measured eight inches in the lateral direction and to simulate O-ring glands of a flight joint, 55-mil ID tubes were attached to the sides of the test article. This set-up allowed for flow impingement inside the detail section of the assembly and traversal of gas flow in two lateral directions. The tubes were 5 feet long, made of stainless steel, and had fill bottles attached to the end. The fill bottles contained the additional free volume necessary to match the free volume contained in a flight-configured joint-4. Original intent of the tubing was to simulate flow friction and heat transfer associated with a pressurizing gland.

Delivered environments were consistent with inlet pressure measurements averaging ~200 psia. Several attempts were made at measurement of inlet gas temperature but were generally considered unsuccessful. The test article grain was cast from shuttle propellant TP-H1148 thus theoretical flame temperatures and combustion

gas thermochemistry was considered comparable to flight. Details of hardware, measurements and results are found in Ref. [3].

The following section provides a brief description of the test configuration followed by a comparison of analysis results versus test measured data.

Configuration-1

The leak path was machined and width fixed at 150 mils confined to the primary gland. Gaps along the path ranged from 50-60 mil, at the entrance, to 30-40 mils adjacent to the gland. Total volume was ~3.8 in^3. Shown in Fig. 5-7 are predicted and measured pressures, temperatures and erosion.
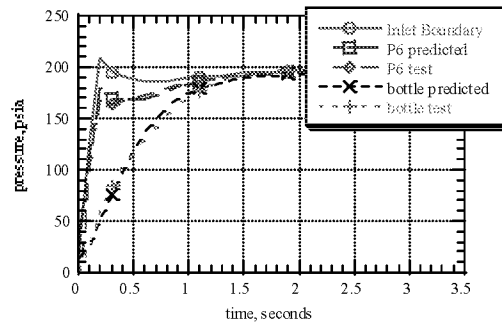

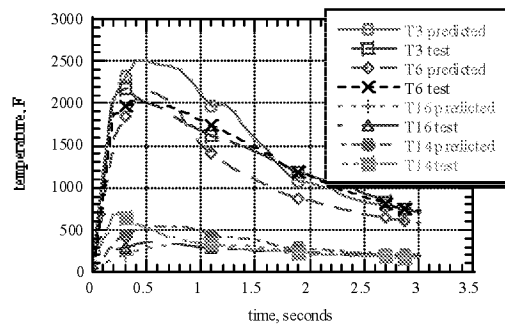Fig. 5. Configuration-1, Leak Path and Fill Bottle Pressure Comparison

Fig. 6. Configuration-1, Leak Path Gas and Metal Temperature Comparison
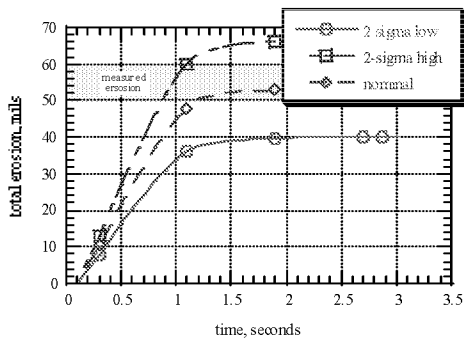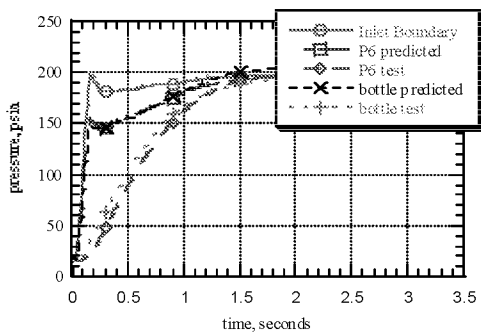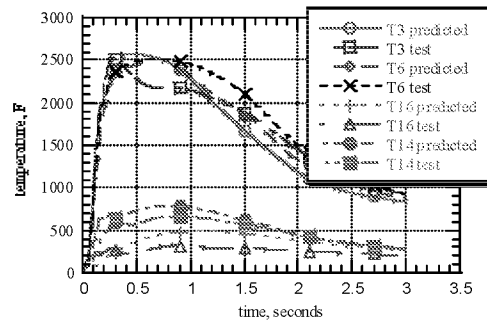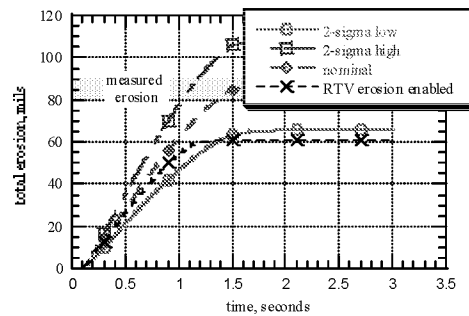
5

Fig. 7. Configuration-1, Primary O-ring
Erosion Comparison

Pressure transients, thermocouple data and primary seal erosions compare well. There is generally less than 20% error in the predicted versus measured temperatures. Nominal erosion prediction was within scatter of measured erosion.

Configurations-2,6

Fill volumes and inlet gaps are nominal. Path width has been reduced to 100 mils. Configuration-6 uses an RTV formed inlet. Provided in Figs. 8-10 are results for test configuration-2. Fig. 10 shows the nominal erosion for configuration–6.

Fig. 8. Configuration-2, Leak Path and Fill
Bottle Pressure Comparison

Fig. 9. Configuration-2, Leak Path Gas and
Metal Temperature Comparison

Fig. 10. Configuration-2/6, Primary O-Ring
Erosion Comparison

Pressure transients, thermocouple data and seal erosions compare well. In-depth bond line temperatures are cooler than predicted but gas temperature comparison is good. Nominal erosion prediction was within scatter of measured erosion.

Confgiurations-3,4,11,14

For these configurations leg-3 is open in the lateral direction. Joint gaps and fill volumes are nominal. Varied were leg-1/2 widths and path materials. Two tests with 150 mil inlet (one machined and one RTV'ed) and two tests with a 100 mil inlet. All results for these cases are similar - thus comparisons for only one configuration are presented. Shown in Figs. 11-13 are results for configuration-4.
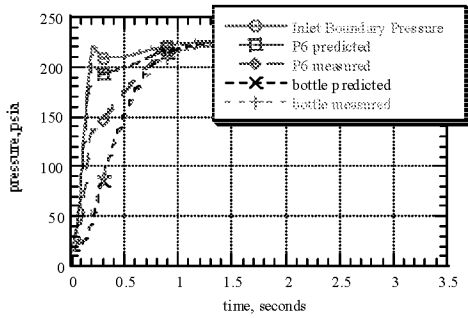
Fig. 11. Configuration-4, Leak Path and Fill
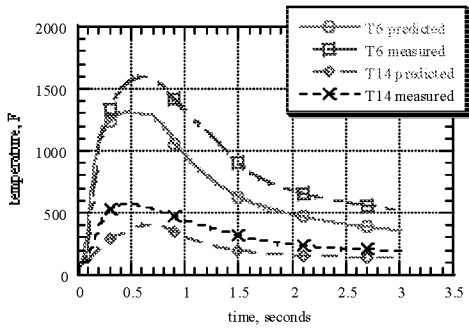Bottle Pressure Comparison

Fig. 12. Configuration-4, Leak Path Gas and
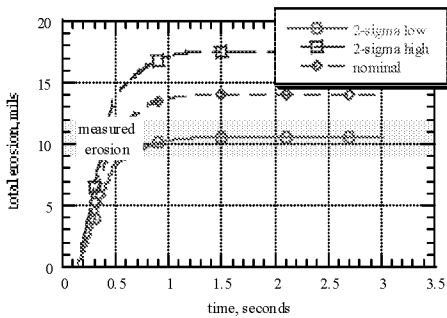Metal Temperature Comparison

Fig. 13. Configuration-4, Primary O-Ring
Erosion Comparison

For the unconfined cases predicted bottle
pressures compare well, implying that computed
mass flow rates are accurate. Centerline pressures
in leg-3 did not compare well. Temperature
predictions were generally lower than measured
by 20-40%. The lower 2-σ erosion prediction is
the best match with the measured data.

Secondary Gland Filling Cases

Four tests were conducted with a flawed
primary seal, allowing pressurization of the
chamfer and secondary gland. Results for
configuration-8 are presented. Geometry is
similar to a flight-configured joint-4 and
measurable secondary O-ring erosion was
produced. Configuration-8 had a confined 150
mil machined path to the primary. The primary
seal had a "dog-bone" defect aligned with the
inlet path. Fill volume for the primary gland was
nominal. The chamfer contained ~5.41 in^3 and
secondary ~4.21 in^3. Leading into the secondary
gland, the metal gap measured 5 mils. Shown in
Figs. 14-17 are comparisons for bottle pressures,
inlet gas/metal housing temperatures and
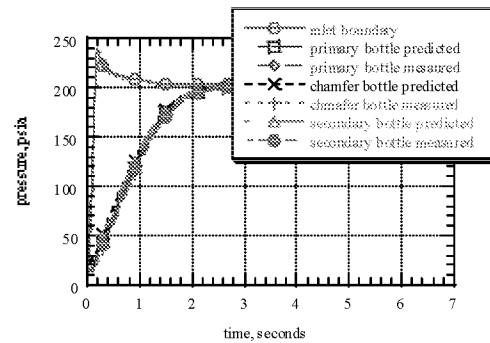secondary O-ring erosion.

Fig. 14. Configuration-8, Secondary Gland Case
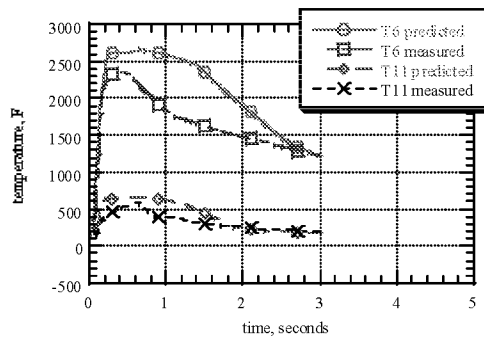Fill Bottle Pressure Comparison

Fig. 15. Configuration-8, Secondary Gland Case
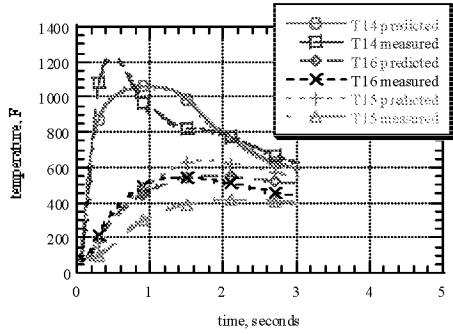Gas Temperature Comparison

7

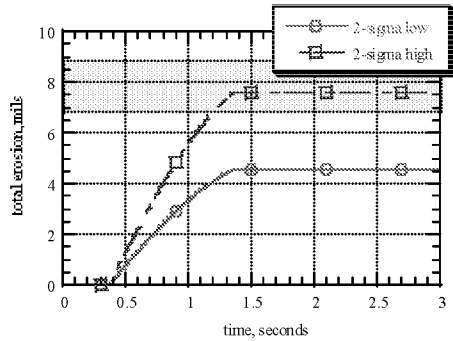Fig. 16. Configuration-8, Secondary Gland Case
Metal Temperature Comparison

Fig. 17. Configuration-8, Secondary Gland Case
Secondary O-ring Erosion Comparison

Flight Configured Joint Modeling

To account for differences between the test article and full-scale joint, the following modeling modifications were made. Effective joint-4 gland flow areas, hydraulic diameters, flow path lengths and volumes were calculated using current configuration data. These calculations accounted for curvature of a seated O-ring and effect of assembly grease. Full-scale nozzle environments adjusted for the joint-4 location were used. Early in motor operation static pressures at the joint are ~150 psia. A temperature of 5100°R was assumed for gas available for pressurization. Standard chamber data was used for adjustment of local pressure and temperature as a function of time.

Two cases were investigated. The first assumes a pre-existing leak path to the secondary at motor ignition. Geometry of the leak path was the same as test configuration-8. For this case, pressures, temperatures and secondary seal total erosion is presented. The second case deals with the smart void scenario. Analysis begins at 104 seconds when the char line has penetrated the first turn and exposes a smart void. For this case, pressures, temperatures and primary seal erosions are presented for various leak path widths.

Provided in Figs. 18-20 are results for the secondary gland pressurization. The analysis assumes a 150 mil leak path and 150 mil dog-bone in the primary at motor ignition.
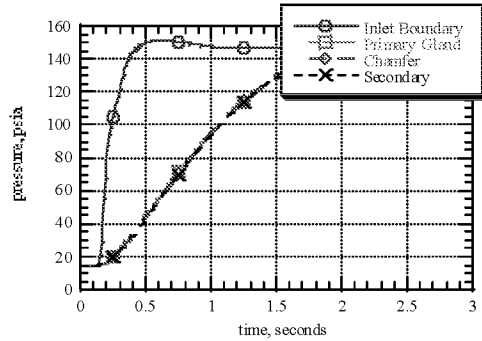

Fig. 18. Leak Path to Secondary @ Ignition
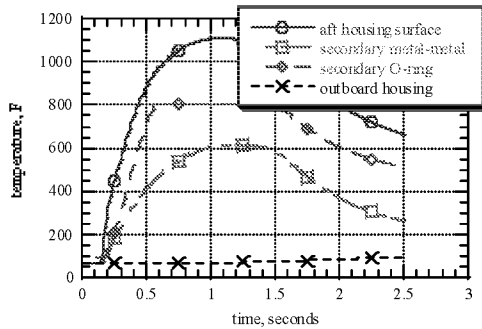Flight Case Gland Pressures

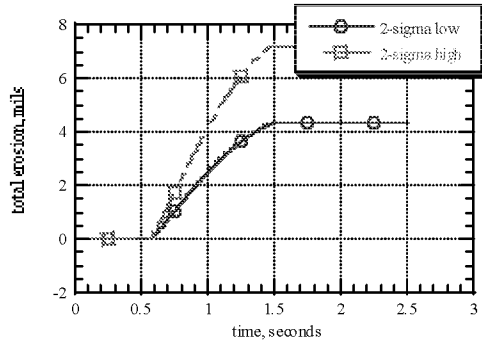Fig. 19. Gas Path to Secondary @ Ignition
Flight Case Temperatures

Fig. 20. Gas Path to Secondary @ Ignition
Secondary O-ring Erosion

Gland pressure response is similar to test results. The joint volume fill time is ~3 seconds. Metal surface temperatures adjacent to the gas path range from 1100°F next to the primary to 600°F in the secondary metal gap. Outboard surfaces

8

remain ambient. Secondary seal erosion is predicted to be 5 mils.

Shown in Figs. 21-23 are parametric results for primary gland pressurization assuming a 30, 50 and 100 mil smart void. Inlet pressures are approximately 80 psia. Filling of the gland occurs in less than two seconds for all cases. Peak housing temperatures are generally less than 500°F for all cases. Maximum primary seal erosion of 20 mils is predicted with a 50 mil leak path.
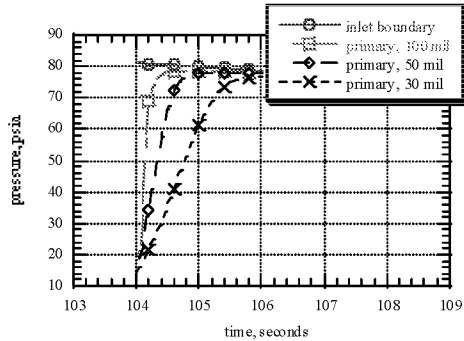

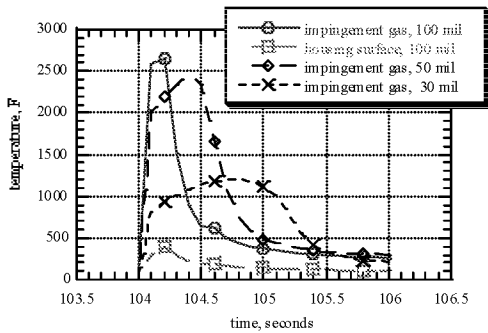Fig. 21. Smart Void Case, Predicted Primary Gland Pressures

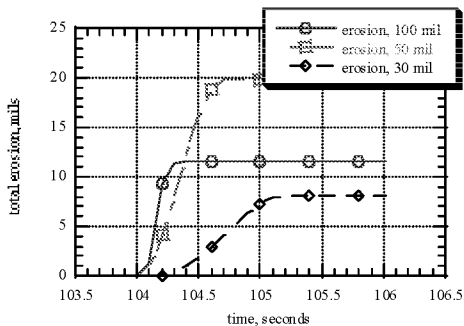Fig. 22. Smart Void Case, Predicted Gas And Metal Temperatures

Fig. 23. Smart Void Case, Predicted Primary Seal Erosion

Conclusions

Based on results presented in this study, the following conclusions / observations are made;

(1) Test configurations-1,-2 provided calibration benchmarks for inlet gas temperature. By machining the leak path, flow areas remained constant over time. There was no flow spreading to be accounted for in determination of mass velocities at the jet origin. These configurations provided the least amount of guesswork in quantifying the effect of impingement gas temperature on seal erosion. Inlet gas temperature of ~5100°R gave the best fit to erosion and thermocouple data.

(2) Methodologies used for prediction of fill bottle pressurization rates were accurate without use of empirically derived factors to account for comparison mismatches. The gas flow network global method of solution provided good estimates of total mass flow and hence a solid basis for the sub-model procedures used.

(3) Temperature comparisons were acceptable given the nature of the measurements, e.g., large gradients, tiny gaps and millisecond time scales. Gas temperature measurements were difficult to match and required sub-modeling of the thermocouple junction. Sub-model results indicate gas temperatures may be in error as much as 1000°F during peak flow rate conditions.

(4) Seal erosion predictions were in good agreement for the confined jet cases. Erosion coefficients for a planar jet[9] best fit the measured data. Nominal predictions usually were bounded within the scatter of the data. The impingement film coefficient relationships contained in Ref. [6] were slightly modified to account for 2-D velocity decay dependencies.

(5) Largest comparison inaccuracies occurred in non-confined geometry where the flow field is multidimensional and CFD sub-modeling required. The analysis tendency was to over-predict seal erosions with CFD computed flow fractions. Based on nominal geometry, the fractions were reduced by a factor of 2-3 to best fit the data. Parametric CFD analyses shows that varying the

secondary metal gap from the nominal 5 mils to 3 mils yields approximately the right magnitude for the flow fraction. The over-prediction tendency may be an artifact of assembly tolerances or soot / condensable deposition all of which contribute to off-nominal geometry.

(6) Primary O-ring erosion for all "unconfined" configurations ranged between 5 and 12 mils. Model results suggest that venting leg-3 complete circumference and adding this volume back into total system volume would result in double the primary erosion (10-25 mil range). Model response indicated peak flow rate magnitudes remained about the same, occurred at the same time but fill times increased. The time increase was proportional to the volume increase, which was proportional to the erosion increase (about double). Recall the 100 mil confined test produced seal erosion on the order of 90-100 mils, about 10 times the erosion amount of the spreading cases. This observation suggests that a vented leg-3 is more tolerant of seal erosion in the worst case scenarios.

(7) The issue of inlet leak path width and what is considered "worst case" was assessed. For the smart void case, it was determined that a maximum primary seal erosion of 20 mils occurred with a 40-50 mil initial leak path size. Below this threshold, total erosions decreased as a function of decreased width. Albeit fill times are longer, decreasing impingement gas temperatures are controlling seal erosion rates at the smaller gas path widths.

(8) Test results provided in ETP-1385 are conservative due to the following; test free volumes were larger, gland geometry more constrictive and source pressures were high. The results are non-conservative due to the lack of testing at smaller leak path widths. Parametrics were performed to evaluate the relationship between inlet leak path width and secondary seal erosion. Findings indicate a maximum secondary erosion of 16 mils occurs at path widths of 40-50 mils. Again, as path widths decrease below 40 mils, gas temperature reduction effects on seal erosion rate control total erosion and not the overall fill time.

References

1. "Joint Pressurization Routine (JPR) Theoretical Development and Users Manual", J. Louie Clayton, NASA-MSFC Internal Memorandum, ED66 (95-01), 1995

2. Systems Improved Numerical Differencing Analyzer (SINDA), J.D. Gaski, Network Analysis Associates Inc., Version 1.8

3. "Tortuous Path Thermal Analysis Test Bed ETP-1385", Thiokol Corporation final report TWR-66623, Mar-04, 1999

4. "Isothermal And Adiabatic flow of Compressible Fluids", C.E. Lapple, American Institute of Chemical Engineers, 1963

5. MSC/PATRAN, Version 7.5, McNeal Scheinidler Corporation, Cosa Mesa California, 1998

6. "O-Ring2: Volume Filling And O-ring Prediction Code, Improved Model Description And Validation, Part I Improved O-ring Erosion Model", M. O'Mally, Thiokol Corporation TWR—17030, 1988

7. "Boundary Layer Theory", Herman Schlichting, Seventh Edition, McGraw Hill Book Company, 1979

8. Finite Difference Navier-Stokes (FDNS3D), CFD code, Y.S. Chen, NASA contract NAS8-37408, 1990

9. "Prediction of Pressurization and Erosion of the SRB O-Rings During Motor Ignition (Part II): Parametric Studies of Field and Nozzle Joints, M. Salita, Thiokol Corporation TWR-15186, July 1985